ADVANCED THEORY AND SIMULATIONS
www.advtheorysimul.com

First-Principles Investigation of Phase Stability in Substoichiometric Zirconium Carbide under High Pressure

*Scott D. Thiel and James P. S. Walsh**

NaCl-type carbides of the early transition metals can exhibit a substantial sub-stoichiometry at the carbon site, impacting a host of bulk properties that depend upon carbon concentration including melting points, mechanical and elastic properties, and superconducting transition temperatures. Unfortunately, control over vacancies remains challenging with current preparation methods, motivating the search for new synthetic approaches that will allow for the prescription of specific vacancy configurations. Here, density functional theory is augmented with alloy cluster expansion to examine the structure and zero kelvin enthalpy of millions of structures across composition and pressure space. The results are used to examine how extreme pressures might be used to access novel ordered and disordered phases of ZrC, many of which have been calculated to be thermodynamically stable yet remain synthetically elusive. High pressure is shown to significantly reduce sub-stoichiometry and drive the system toward fully stoichiometric ZrC. They examine the root of these changes and find that pressure exerts an influence over the distribution and abundance of specific nearest-neighbor vacancy pairs. These results suggest that pressure is a powerful tool for the control of vacancies, and can offer a new synthetic handle on the bulk properties exhibited in this industrially important class of materials.

1. Introduction

Transition metal carbides (TMCs) have been the subject of intense research over the last several decades on account of their outstanding mechanical and chemical properties, with their low compressibilities, high melting points, robust corrosion resistance, and high electrical conductivity making them useful across a number of high-resilience applications. Examples include WC, whose hardness makes it useful in deep earth drilling, and ZrC, whose low nuclear cross section and resistance to fission products attack makes it an ideal coating for fuel particles in high temperature nuclear reactors.[1–3] TMCs have also been investigated as catalysts for hydrogen evolution and deoxygenation,[4–7] energy storage materials,[8–10] and as superconductors.[11–13]

S. D. Thiel, J. P. S. Walsh
Department of Chemistry
University of Massachusetts Amherst
Amherst, MA 01003, USA
E-mail: jpswalsh@umass.edu

The ORCID identification number(s) for the author(s) of this article can be found under https://doi.org/10.1002/adts.202200439

DOI: 10.1002/adts.202200439

TMCs resulting from the Group 4 (Ti, Zr, Hf) and Group 5 (V, Nb, Ta) transition metals tend to adopt the simple cubic rocksalt (NaCl-type) structure, where the metal and carbon atoms exclusively occupy separate fcc sublattices. The carbon atoms can be viewed as interstitial atoms occupying the octahedral spaces between the atoms of the metal lattice (**Figure 1**). This arrangement leads to a very high degree of metal–carbon bonding, which is believed to contribute to their exceptional resilience properties.[14–16] Although the metal sublattice is usually fully occupied, the carbon sublattice can host a wide range of vacancies—up to 50% of the total sites in some cases—while leaving the rest of the structure stable and for the most part unchanged.[17–24] This property is known as sub-stoichiometry, and it plays a vital role in determining bulk properties across many material classes.[25–28]

While the presence of vacancies in the dilute limit ($\approx 10^{-3}$) is usually not sufficient to significantly influence most bulk properties, the concentration of vacancies possible in sub-stoichiometric materials ($\approx 10^{-1}$) can impart quite considerable effects. For example, vacancy concentration correlates to hardness,[14,29,30] thermal conductivity,[31,32] ionic diffusion,[33,34] and electrical conductivity.[34,35]

The carbon sublattice is usually viewed as a solid solution of carbon and vacancies. However, it is also possible for the vacancies to exhibit ordering, which can manifest as the formation of a layered compound (e.g. vacancies forming 2D sheets) or some other distinct stoichiometric compound with a larger unit cell and strong internal order.[20,36,37] Vacancies can also exhibit partial ordering, where some vacancy features are distributed differently than others. A useful way to quantify this distribution is through the use of a radial distribution function, or through other similar functions within the same family such as the pair distribution function (PDF). The PDF gives the probability of finding a particle at a certain distance from a given particle, and thus describes the pairwise distribution of all particles within a system. This type of analysis opens the door to studies that correlate bulk properties to not only the vacancy concentration, but also the distribution patterns of the vacancies.

The observation that NaCl-type carbides only form for Groups 4 and 5 metals has been rationalized on the basis of the energies involved in forming carbon interstitials. It is generally

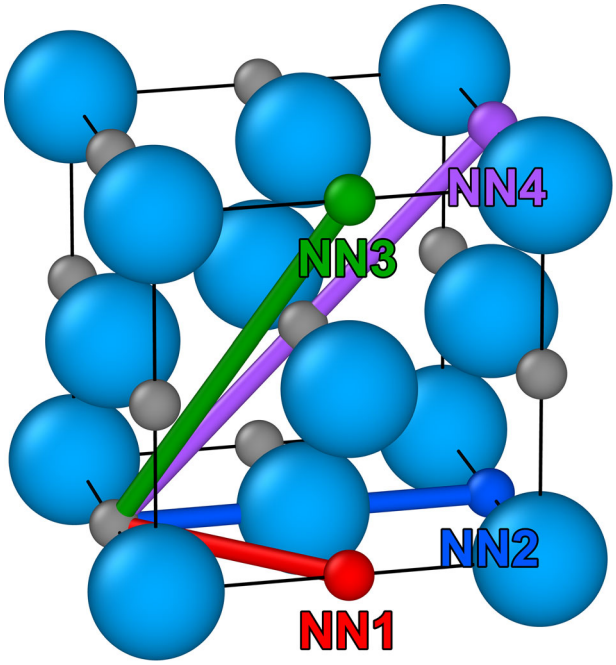

Figure 1. The conventional cell of the cubic rocksalt (NaCl-type) structure of ZrC with the four carbon nearest neighbor distances (NN1, NN2, NN3, and NN4) highlighted in separate colors. The larger blue atoms are zirconium, and the smaller dark gray atoms are carbon. The nearest neighbors are shown from the carbon at $(0, \frac{1}{2}, 0)$.

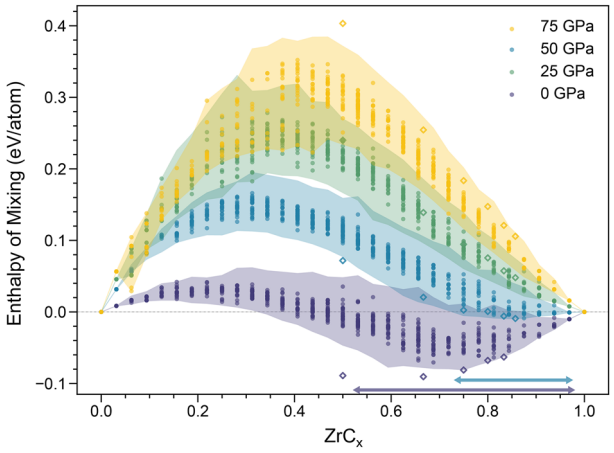

Figure 2. The mixing enthalpy per atom of random ZrC_x structures is plotted against composition. Data is plotted at each pressure of 0, 25, 50, and 75 GPa. The solid circles are random DFT relaxed structures. The shaded areas are the boundaries of the energies of millions of random structures predicted by the CE method. The open diamonds are ordered structures from ground state searches reported elsewhere.[41] At $x = 0$, Zr is in the fcc phase. The experimental stability range at 0 GPa is shown by the purple line above the x-axis. The potential stability range at 25 GPa is shown by the blue line above the x-axis. The green (50 GPa) and yellow (75 GPa) shaded regions for $x < 0.5$ are limited in accuracy indicated by the bottom panels in Figure 3.

accepted that the overall stability of TMCs arises from a delicate balance of M–M and M–C interactions, and that for Group 6 and higher, the overall energetic penalty for the formation of an octahedrally coordinated interstitial is simply too high.[38,39] This precludes the formation of NaCl-type compounds entirely, and leads instead to structurally distinct compounds such as WC and Fe_3C, wherein the carbon occupies a trigonal prismatic environment. The same rationale can be used to explain the observation of sub-stoichiometry: the energetic competition between carbon sites and vacancies leads to a minimum at a specific metal:carbon ratio.

We decided to explore the effect that pressure has on the energies involved in vacancy formation, motivated by the desire to use pressure as a synthetic handle to tune the carbon concentration—and thereby bulk properties that depend upon this concentration—in transition metal carbides. Herein, we use first-principles calculations coupled with cluster expansion machine learning methods to survey how both the overall stability and the vacancy distribution in NaCl-type zirconium carbide evolve with pressure.

2. Results and Discussion

2.1. Thermodynamic Phase Stability of ZrC_x

The mixing enthalpies derived from density functional theory (DFT) calculations for each composition and pressure are plotted as solid points in **Figure 2**. The bounds of the mixing enthalpies for the millions of structures predicted by the cluster expansion (CE) are also shown, and are shaded with the matching colors. The 0 GPa data are in good agreement with experimental observations that ZrC_x is stable around $0.5 \leq x \leq 1.0$ at ambient pressures.[19,40] A selection of ordered structures have been included from ground state searches reported in other work,[41] and they are plotted as open diamonds in Figure 2. It is apparent from a comparison of the datasets that overall pressure works to increase the mixing enthalpy of the ZrC_x system, effectively suppressing substoichiometry at high pressures (50 and 75 GPa). At the intermediate pressure of 25 GPa, we observe that although the bulk of the structures have a positive mixing enthalpy, there remains a subset of the structures which have negative mixing enthalpy and a minimum at a composition distinctly different from that observed at 0 GPa. The composition range of these negative-enthalpy structures is $0.73 \leq x \leq 1.0$. This is promising, as it indicates that pressure could be a potential method for controlling substoichiometry at conditions accessible with large volume press methods.

Ordered phases are plotted as open diamonds in Figure 2. Although these ordered phases appear to lie on the convex hull, only the $Fd\bar{3}m$ Zr_2C ordered phase has been consistently identified through experiment.[40,42–49] There are a few proposed reasons for why Zr_2C is the only ordered phase that can be reliably synthesized, including the possibility that the disordered phases are kinetically "frozen in" during quenching from high temperature synthesis at higher values of x, or that the Zr_2C structure simply outcompetes the other predicted structures, whether that be thermodynamically or kinetically.[49]

Figure 2 shows that by 25 GPa, the mixing enthalpy of the Zr_2C structure has become positive, and therefore is no longer on the convex hull. However, some of the ordered phases at higher values of x retain a negative mixing enthalpy. This suggests that these ordered phases may become more competitive than Zr_2C

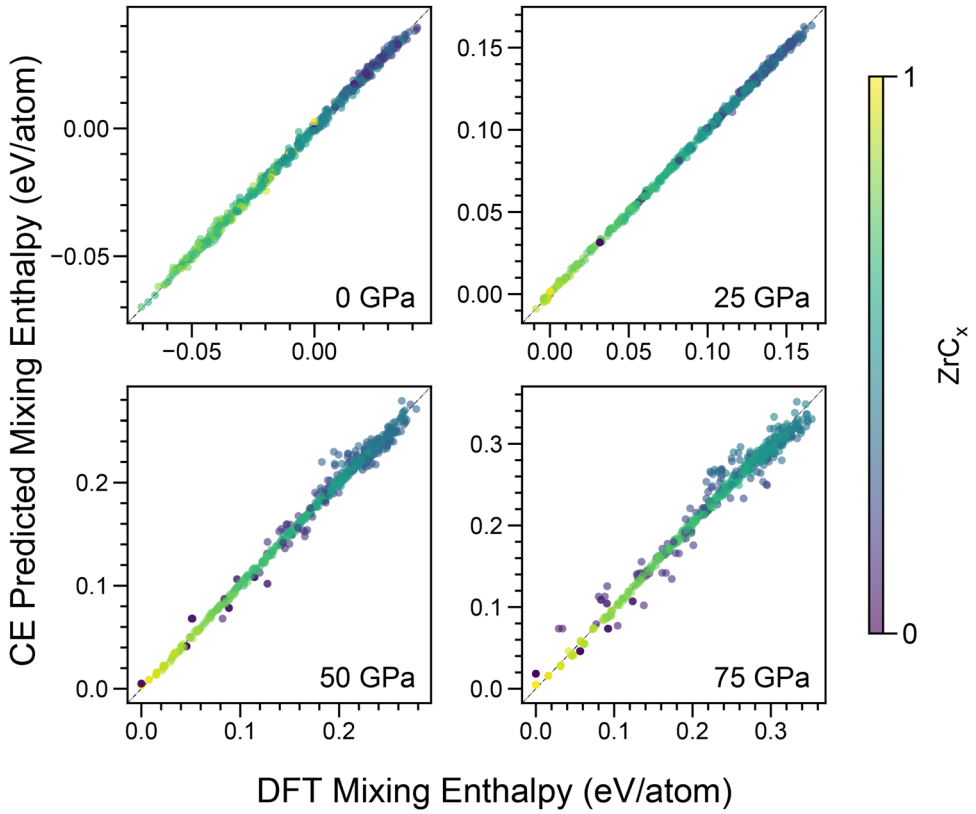

Figure 3. Scatter data for the validation of the CE model is plotted at each pressure. The 0 GPa data shows a very good fit for all compositions with a RMSE of 1.58 meV atom^{-1}. The accuracy at smaller carbon fractions decreases for the higher pressure models, with 75 GPa being the worst with an RMSE of 12.7 meV atom^{-1}. This limits the accuracy in the green (50 GPa) and yellow (75 GPa) shaded regions for $x < 0.5$ in Figure 2. However, the 75 GPa model still shows to be very accurate for fractions $x > 0.5$.

between 0–25 GPa, and could be experimentally targeted with higher pressures.

At the highest pressure of 75 GPa where substoichiometry is effectively driven out of the ZrC system, the mixing enthalpy of the ordered structures is higher than the majority of the disordered structures. This is explained by the significant contribution of thermodynamic work at high pressures, where the $p\Delta V$ term becomes dominant, similar to how entropy dominates the Gibbs free energy at high temperatures. The ordered structures are typically found to have larger unit cell volumes, both in calculation and in experiment,[45,46,50] which leads to them being disfavored compared to the more dense disordered arrangements at higher pressures. This could help to explain the success of hot pressing in achieving dense ZrC with a high carbon occupancy,[51,52] albeit at much lower pressures than examined here.

2.2. Vacancy Distribution Statistics of ZrC_x

The CE method is a form of regression analysis that uses a model constructed from a linear combination of multi-body terms to approximate a property for a given input structure. The model takes as input the occupancy configuration of a lattice or sub-lattice, which in this case is the vacancy configuration of the carbon sublattice. This configuration encodes the concentration and spatial arrangement of vacancies, and so serves as an ideal method for analyzing and extrapolating the effect that vacancy configurations have on the energy of a structure.

The CE is able to yield mixing enthalpies of structures roughly four to five orders of magnitude faster than DFT while maintaining an accuracy around 2 meV atom^{-1} in the relevant phase space. As a result, hundreds of thousands of structures can be processed in a relatively short amount of time, making it feasible to examine the statistical tendencies of these systems on a large scale. Much work has been carried out on ground state structures in an effort to uncover which phases define the convex hull of the ZrC system, and to understand what contributes to the ordering of such structures. However, given that many experiments have reported disordered ZrC phases, combined with the fact that the convex hull is flat above 25 GPa, we opted to investigate how vacancy pairs are distributed among the full range of configuration space. The CE was used to sample around one million random configurations of supercells containing 32 Zr sites at each pressure. **Figure 3** shows the scatter data used to validate the CEs. The 0 and 25 GPa models shows excellent accuracy to DFT data across the entire composition range. The 50 and 75 GPa models show deviation from DFT data at low compositions, but remain remarkably accurate for higher compositions. We find this satisfactory since the structures of interest will be those with higher carbon compositions (Figure 2).

In order to investigate the energetic spread of the various possible vacancy arrangements—and thus to assess which arrange-

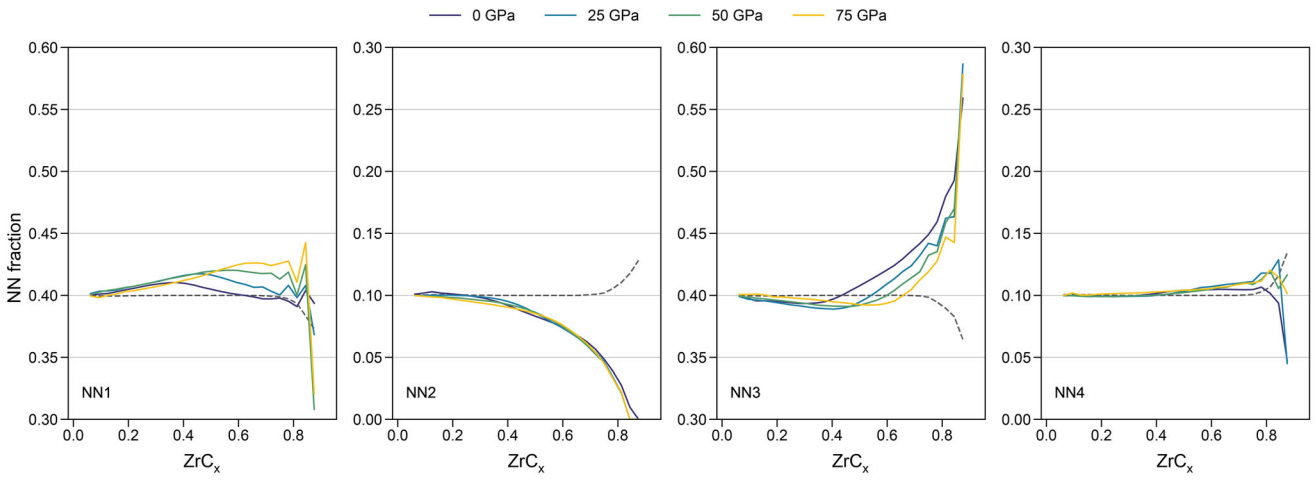

Figure 4. Nearest neighbor vacancy fractions for the lower quarter of mixing enthalpy (Q1, stable) among each composition at different pressures. Nearest neighbors are split into separate views for visual clarity. Higher values of NN fractions correspond to a higher concentration of that particular feature (NN pair). The dashed gray line represents the NN fractions of over the full range of predicted structures to serve as a reference line.

ments are more likely to appear in the disordered structures—we grouped the structures based on their quantiles of mixing enthalpy. For example, structures in the bottom quarter (Q1) have their mixing enthalpy falling below the first quartile and make up the bottom 25% of structures by mixing enthalpy for their respective composition.

While configurations can be characterized by the positions of their vacancies—or more simply as a "spin" vector of the vacancies as used in the CE method—it can be more useful to distill down to the number of nearest-neighbor (NN) pairs present in the calculation cells. While this is not a complete description of the distribution of vacancies, it nevertheless serves as a way to correlate our observations to clear and distinct structural features. These counts of NN pairs are effectively an analogue for pair/radial distribution functions, and for structures where the atoms are on ideal lattice positions it obviates pulling a distribution where no distribution exists. We standardize these NN counts by composition and stability group (Q1, Q2, etc.) so that the resulting NN fraction is the relative contribution of that NN pair to the total spread of NN pairs. For example, the NN1 fraction at a given composition is the number of NN1 pairs present at that composition divided by the sum of NN1, NN2, NN3, and NN4 pairs present at that same composition. This normalization allows the NN counts to be more easily compared across composition, where otherwise compositions with more vacancies would have larger NN counts on account of there being more vacancy pairs in general.

The nearest neighbor analysis of vacancy pairs in Q1 (lower quarter) structures is shown in **Figure 4**. The dashed gray line is the NN fraction computed over the full range of predicted structures over all pressures (i.e., without being partitioned into stability groups). This line serves as a reference against which to compare the NN fractions within each stability group, and allows us to examine how the concentration of nearest neighbor pairs in stable structure differs from that in completely random structures. As we approach $x = 0$, all NN fractions converge with the reference value since there are no more degrees of freedom when the carbon atoms are fully removed.

For most NN pairs, we begin to observe significant departures from the reference trace as x surpasses 0.5. In NN1, the traces are together above the reference trace and split up around $x = 0.4$ where the 0 GPa trace approaches the reference trace. For $0.5 < x < 0.8$, the NN3 and NN4 pairs both start to become more abundant than the reference value, while NN2 becomes drastically less abundant. In the same region, the NN1 traces are at their most spread out much like the NN3 traces. We can reduce these differences into a convenient value for comparison by determining the average difference of the NN fraction from reference over the $0.5 < x < 0.8$ composition range. For the NN2 pairs, we see a difference of around −0.035 at all four pressures examined. For NN3 pairs, we see that the largest difference is observed at 0 GPa, where the data averages to +0.030 relative to the reference. In contrast, for the NN1 pairs, the largest difference is observed at 75 GPa, where the data averages to +0.025 above the reference. We can strengthen our notion of "stable" by also considering the NN fractions under the more strict metrics of the bottom fifth and first percentiles of mixing enthalpy. These metrics show the same qualifying features, and in fact are even more pronounced. See the Supporting Information for plots with these metrics.

We can further investigate the chemistry of these vacancy pairs within the context of the energy associated with forming them. These energies, called interaction energies, can be calculated using Equation (1) and are plotted in **Figure 5**. The vacancy interaction energies at 0 GPa are consistent with the ordering of those reported by others for this system.[50,53,54] Intuitively, one should expect the lower energy (more stable) structures to contain a greater concentration of the lower energy interactions, and a lower concentration of the higher energy interactions. This trend has been observed in theoretical ground state ZrC structures in other work,[53] and we observe this to be the case for our bulk random structures. The NN3 pair has the lowest interaction energy, which explains why it has the largest difference above the reference line, while the NN2 pair has by far the highest interaction energy, which is consistent with it being the furthest below the reference line. Further support for this correlation can be seen in an examination of unstable Q4 (highest 25%) structures,

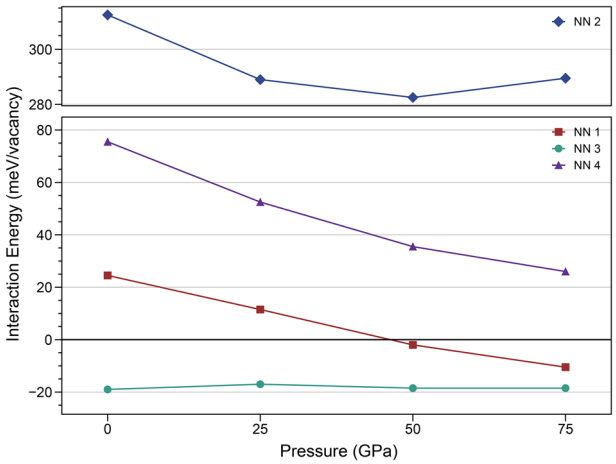

Figure 5. Interaction energies of nearest neighbor pairs plotted as a function of pressure. Interactions show the preference NN3 > NN1 > NN4 > NN2 for the full pressure range 0–75 GPa. The NN1 interaction energy approaches the energy of the NN3 interaction, crossing from positive formation to negative formation around 50 GPa. The NN2 interaction turns to increase at a pressure of 75 GPa indicating a more complex change to the potential energy surface at very high pressures. The NN3 interaction remains effectively constant, with variations below 2 meV—close to the uncertainty in the calculations.

which show enhanced fractions for the unstable interactions (see Supporting Information).

Our data allows us to extend this analysis to higher pressures, where we observe a number of interesting trends. NN1, NN2, and NN4 all show a significant dependence on pressure, while NN3 shows effectively none. For the NN pairs that show a dependence on pressure, the interaction energy decreases in all cases up to 50 GPa. At the highest pressure of 75 GPa, the energy for the NN1 pair interaction actually becomes negative, having dropped 35 meV from its 0 GPa energy. The energy of the NN4 pair interaction also drops by about 50 meV over the examined pressure range. The NN2 pair begins to rise in energy at 75 GPa, but overall remains significantly higher in energy than the other NN pairs. These changes to the relative energies correlate with the observed changes in the NN fractions. For example, it explains why the fraction of NN1 pairs is increased at the expense of NN3 pairs upon increasing pressure. Indeed, the difference in the pressure dependence of the various NN pairs can be viewed as the source of the pressure dependence observed in the vacancy distributions.

3. Conclusion

We have used DFT and cluster expansion methods to show that pressure has a significant impact upon not only the vacancy concentration in zirconium carbide, but also the spatial distribution of those vacancies. Large changes to the thermodynamic stability at 0 K are observed even at pressures as low as 25 GPa, opening up new opportunities for the targeting of ordered phases in the Zr–C system under synthetically accessible pressures. As these calculations are all performed at 0 K, they do not take into account the effect of finite temperature. At temperatures upward of 1200 K, which are typically required for ZrC syntheses, the synthesis of ordered phases may be difficult. This may still be the case even at 25 GPa where the pV term in the enthalpy is expected to be significant. Thermal quenching at this pressure would likely result in disordered phases. However, slow cooling under high pressure may open a route to the discovery of new phases in this system.

We have also demonstrated how pressure influences the vacancy interaction energies, which correlate well with the ordering and vacancy distribution in ZrC. This presents a new avenue for accessing different ordered and disordered configurations of substoichiometric transition metal carbides through pressure-controlled defect engineering, where relative vacancy interaction energies can be used to tune vacancy distribution.

These results provide a foundation for experimental investigations of the relationship between vacancy distribution and bulk properties in other early transition metal carbides. For example, the superconducting critical temperatures in NaCl-type TaC and NbC have been shown to increase as the fraction of carbon approaches unity. Thus, high-pressure synthesis may serve as a powerful tool to enhance superconductivity in both known and as-yet undiscovered transition metal carbides.

4. Experimental Section

First-Principles DFT Calculations: First-principles DFT calculations were performed using `CASTEP` v19.11.[55] All calculations used the Perdew–Burke–Ernzerhof approach to the generalized gradient approximation of the exchange-correlation functional.[56] This functional should produce reliable high pressure equilibrium structures at an acceptable cost.[57–59] Geometry relaxations where the cell parameters were allowed to vary were treated with a finite basis correction implemented in the CASTEP code. Calculations used for fitting the cluster expansion were performed with a Monkhorst–Pack[60] grid spacing of at least 0.05 $Å^{-1}$ and a cutoff energy of 620 eV. The pseudopotentials were generated using the QC5 setting for CASTEP's on-the-fly generated psudopotentials, which produced potentials optimized for high-throughput calculations.[55] The calculation cells were generated by randomly removing a number of carbon atoms from a cubic supercell of 32 ZrC formula units with the aid of the atomic simulation environment (`ASE`) python package.[61] This supercell was the $2 \times 2 \times 2$ tiling of the conventional cell. The numbers of carbon atoms to remove were chosen randomly from a modified normal distribution. Mixing enthalpies were calculated as the formation of NaCl-type ZrC_x from the end members of the composition space.

Interaction energies were determined from total energies calculated from first-principles methods using `CASTEP`. Supercells of $3 \times 3 \times 3$ conventional cells, corresponding to 108 formula units, of ZrC were used for the vacancy pairs. The calculations used a Monkhorst–Pack grid spacing of 0.02 $Å^{-1}$ and a cut-off energy of 680 eV. These parameters were converged to within 0.005 GPa of the calculated stress of defect cells for a balance between cost and accuracy. The potentials used were `CASTEP`'s default on-the-fly generated ultrasoft pseudopotentials. The cells were relaxed such that the defect cells were fixed to the defect free structure with only the ionic positions relaxed. See the Supporting Information for more details. This allowed considering the defects both with the local stress they induce. The interaction energy of a given vacancy pair, E_{pair}, was defined as the difference between: i) one cell containing the vacancy pair, $E(Zr_{108}C_{106})$, plus one vacancy-free cell, $E(Zr_{108}C_{108})$; and ii) two cells containing a single vacancy, $E(Zr_{108}C_{107})$:[62]

$$E_{pair} = \frac{1}{2}[E(Zr_{108}C_{108}) + E(Zr_{108}C_{106}) - 2E(Zr_{108}C_{107})] \quad (1)$$

Cluster Expansion Calculations: The CEs were constructed using the `icet` v1.4[63] package to build and sample CEs, with `ASE` as a supporting framework. All cluster spaces were constructed from NaCl-type ZrC

with lattice parameter $a = 4.5$ Å, and cutoffs of 8, 8, 7, and 6.5 Å for the respective 2-, 3-, 4-, and 5-body interactions. The carbon sub-lattice was treated as a binary solution of carbon atoms and vacancies. Because of the narrow scope of the model, it had no consideration for pressure, and thus it cannot generalize in the pressure dimension. A separate model was therefore constructed for each pressure investigated.

The models were fit to around 550 DFT-relaxed structures from each pressure using the mixing enthalpy (eV atom^{-1}) as the fit key and lasso as the fit method. The model fit was constructed in the same way for each pressure, using 125 parameters and achieving a root mean square error (RMSE) of about 2 meV atom^{-1} for relevant structures. For each pressure investigated, around one million structures were sampled from the CE for a total of over four million structures sampled. Structures to be sampled were generated as supercells of $2 \times 2 \times 2$ conventional cells corresponding to 32 formula units of ZrC. Random configurations were pulled from a normal distribution of carbon vacancies truncated to the interval$^{[2,30]}$ with $\mu = 16$ and $\sigma = 6$.

Supporting Information

Supporting Information is available from the Wiley Online Library or from the author.

Acknowledgements

The authors wish to thank Prof. Ashwin Ramasubramaniam for insightful comments on this work. This work was completed in part with resources provided by the Massachusetts Green High Performance Computing Cluster (MGHPCC). The authors gratefully acknowledge the University of Massachusetts Amherst for startup funding.

Conflict of Interest

The authors declare no conflict of interest.

Data Availability Statement

The data that support the findings of this study are openly available in Zenodo at https://doi.org/10.5281/zenodo.6908605, reference number 6908605.

Keywords

carbides, cluster expansion, DFT calculations, first principles, high pressure

Received: June 21, 2022
Revised: July 27, 2022
Published online: August 19, 2022

[1] A. Motta, K. Sridharan, D. Morgan, I. Szlufarska, USDOE, Nuclear Energy University Programs, USA **2013**, https://doi.org/10.2172/1097003.
[2] Y. Katoh, G. Vasudevamurthy, T. Nozawa, L. L. Snead, *J. Nucl. Mater.* **2013**, *441*, 718.
[3] A. Ul-Hamid, *Mater. Adv.* **2020**, *1*, 988.
[4] X. Zhang, C. Shi, B. Chen, A. N. Kuhn, D. Ma, H. Yang, *Curr. Opin. Chem. Eng.* **2018**, *20*, 68.
[5] M. M. Sullivan, C.-J. Chen, A. Bhan, *Catal. Sci. Technol.* **2016**, *6*, 602.
[6] R. Michalsky, Y.-J. Zhang, A. A. Peterson, *ACS Catal.* **2014**, *4*, 1274.
[7] Q. Gao, W. Zhang, Z. Shi, L. Yang, Y. Tang, *Adv. Mater.* **2018**, *31*, 1802880.
[8] Y. Zhong, X. Xia, F. Shi, J. Zhan, J. Tu, H. J. Fan, *Adv. Sci.* **2016**, *3*, 1500286.
[9] Y. Xiao, J.-Y. Hwang, Y.-K. Sun, *J. Mater. Chem. A* **2016**, *4*, 10379.
[10] B. Anasori, M. R. Lukatskaya, Y. Gogotsi, *Nat. Rev. Mater.* **2017**, *2*, 16098.
[11] R. Willens, E. Buehler, B. Matthias, *Phys. Rev.* **1967**, *159*, 327.
[12] N. Szymanski, I. Khatri, J. Amar, D. Gall, S. Khare, *J. Mater. Chem. C* **2019**, *7*, 12619.
[13] V. Kamysbayev, A. S. Filatov, H. Hu, X. Rui, F. Lagunas, D. Wang, R. F. Klie, D. V. Talapin, *Science* **2020**, *369*, 979.
[14] X.-X. Yu, G. B. Thompson, C. R. Weinberger, *J. Eur. Ceram. Soc.* **2015**, *35*, 95.
[15] S.-H. Jhi, J. Ihm, S. G. Louie, M. L. Cohen, *Nature* **1999**, *399*, 132.
[16] S.-H. Jhi, S. G. Louie, M. L. Cohen, J. Ihm, *Phys. Rev. Lett.* **2001**, *86*, 3348.
[17] J. Billingham, P. S. Bell, M. H. Lewis, *Acta Crystallogr., Sect. A: Found. Adv.* **1972**, *28*, 602.
[18] S. T. Oyama, J. C. Schlatter, J. E. Metcalfe, J. M. Lambert, *Ind. Eng. Chem. Res.* **1988**, *27*, 1639.
[19] C. Gasparrini, D. sham Rana, N. L. Brun, D. Horlait, C. N. Markides, I. Farnan, W. E. Lee, *Sci. Rep.* **2020**, *10*, 6347.
[20] E. Parthé, K. Yvon, *Acta Crystallogr., Sect. B: Struct. Sci., Cryst. Eng. Mater.* **1970**, *26*, 153.
[21] H. W. Hugosson, P. Korzhavyi, U. Jansson, B. Johansson, O. Eriksson, *Phys. Rev. B* **2001**, *63*, 165116.
[22] H. Höchst, R. D. Bringans, P. Steiner, T. Wolf, *Phys. Rev. B* **1982**, *25*, 7183.
[23] S. O. Ganiyu, N. Oturan, S. Raffy, M. Cretin, R. Esmilaire, E. van Hullebusch, G. Esposito, M. A. Oturan, *Water Res.* **2016**, *106*, 171.
[24] J. Rabalais, R. J. Colton, A. M. Guzman, *Chem. Phys. Lett.* **1974**, *29*, 131.
[25] I. Persson, A. el Ghazaly, Q. Tao, J. Halim, S. Kota, V. Darakchieva, J. Palisaitis, M. W. Barsoum, J. Rosen, P. O. Å. Persson, *Small* **2018**, *14*, 1703676.
[26] X. Zang, S. Wang, R. Zhang, *J. Phys. Chem. Lett.* **2021**, *12*, 4434.
[27] Y. Zhu, J. Tafto, M. Suenaga, *MRS Bull.* **1991**, *16*, 54.
[28] C. Park, R. L. Snyder, *J. Am. Ceram. Soc.* **1995**, *78*, 3171.
[29] W. S. Williams, *J. Appl. Phys.* **1964**, *35*, 1329.
[30] K. Balasubramanian, S. V. Khare, D. Gall, *Acta Mater.* **2018**, *152*, 175.
[31] Y. Zhang, B. Liu, J. Wang, J. Wang, *Acta Mater.* **2016**, *111*, 232.
[32] Y. Zhou, W. G. Fahrenholtz, J. Graham, G. E. Hilmas, *J. Mater. Sci. Technol.* **2021**, *82*, 105.
[33] Q. Tang, Z. Zhou, P. Shen, *J. Am. Chem. Soc.* **2012**, *134*, 16909.
[34] W. S. Williams, *Prog. Solid State Chem.* **1971**, *6*, 57.
[35] K. Hantanasirisakul, Y. Gogotsi, *Adv. Mater.* **2018**, *30*, 1804779.
[36] A. Leineweber, H. Jacobs, *J. Alloys Compd.* **2000**, *308*, 178.
[37] A. I. Gusev, *Phys. Status Solidi B* **1991**, *163*, 17.
[38] Q. Wang, K. E. German, A. R. Oganov, H. Dong, O. D. Feya, Y. V. Zubavichus, V. Y. Murzin, *RSC Adv.* **2016**, *6*, 16197.
[39] M. Gren, E. Fransson, M. Ångqvist, P. Erhart, G. Wahnström, *Phys. Rev. Mater.* **2021**, *5*, 033804.
[40] D. Sham, B. K. Rana, E. Z. Solvas, W. E. Lee, I. Farnan, *Sci. Rep.* **2020**, *10*, 3096.
[41] C. Xie, A. R. Oganov, D. Li, T. T. Debela, N. Liu, D. Dong, Q. Zeng, *Phys. Chem. Chem. Phys.* **2016**, *18*, 12299.
[42] H. Goretzki, *Phys. Status Solidi B* **1967**, *20*, K141.
[43] C. H. D. Novion, V. Maurice, *J. Phys. Colloq.* **1977**, *38*, 211.
[44] Y. Karimov, V. Ehm, Y. Khidirov, Y. S. Latergaus, *Izv. Akad. Nauk Uzb. SSR, Ser. Fiz.-Mat. Nauk* **1979**, *11*, 81.

[45] W. Hu, J. Xiang, Y. Zhang, S. Liu, C. Chen, P. Wang, H. Wang, F. Wen, B. Xu, J. He, D. Yu, Y. Tian, Z. Liu, *J. Mater. Res.* **2012**, *27*, 1230.
[46] B. Wei, Y. Wang, H. Zhang, D. Wang, S. Peng, Y. Zhou, *Mater. Lett.* **2018**, *228*, 254.
[47] W. Hu, S. Liu, B. Wen, J. Xiang, F. Wen, B. Xu, J. He, D. Yu, Y. Tian, Z. Liu, *J. Appl. Crystallogr.* **2012**, *46*, 43.
[48] Y. Zhou, T. W. Heitmann, E. Bohannan, J. C. Schaeperkoetter, W. G. Fahrenholtz, G. E. Hilmas, *J. Am. Ceram. Soc.* **2019**, *103*, 2891.
[49] T. Davey, Y. Chen, *Int. J. Ceram. Eng. Sci.* **2022**, *4*, 134.
[50] T. Davey, K. Suzuki, H. Miura, Y. Chen, *RSC Adv.* **2021**, *11*, 32573.
[51] P. Barnier, C. Brodhag, F. Thevenot, *J. Mater. Sci.* **1986**, *21*, 2547.
[52] C. Nachiappan, L. Rangaraj, C. Divakar, V. Jayaram, *J. Am. Ceram. Soc.* **2010**, *93*, 1341.
[53] Y. Zhang, B. Liu, J. Wang, *Sci. Rep.* **2015**, *5*, 18098.
[54] V. I. Razumovskiy, A. V. Ruban, J. Odqvist, P. A. Korzhavyi, *Phys. Rev. B* **2013**, *87*, 054203.
[55] S. J. Clark, M. D. Segall, C. J. Pickard, P. J. Hasnip, M. I. J. Probert, K. Refson, M. C. Payne, *Z. Kristallogr. - Cryst. Mater.* **2005**, *220*, 567.
[56] J. P. Perdew, K. Burke, M. Ernzerhof, *Phys. Rev. Lett.* **1996**, *77*, 3865.
[57] P. Ziesche, S. Kurth, J. P. Perdew, *Comput. Mater. Sci.* **1998**, *11*, 122.
[58] J. E. Jaffe, J. A. Snyder, Z. Lin, A. C. Hess, *Phys. Rev. B* **2000**, *62*, 1660.
[59] C. Stampfl, W. Mannstadt, R. Asahi, A. J. Freeman, *Phys. Rev. B* **2001**, *63*, 155106.
[60] H. J. Monkhorst, J. D. Pack, *Phys. Rev. B* **1976**, *13*, 5188.
[61] A. H. Larsen, J. J. Mortensen, J. Blomqvist, I. E. Castelli, R. Christensen, M. Dułak, J. Friis, M. N. Groves, B. Hammer, C. Hargus, E. D. Hermes, P. C. Jennings, P. B. Jensen, J. Kermode, J. R. Kitchin, E. L. Kolsbjerg, J. Kubal, K. Kaasbjerg, S. Lysgaard, J. B. Maronsson, T. Maxson, T. Olsen, L. Pastewka, A. Peterson, C. Rostgaard, J. Schiøtz, O. Schütt, M. Strange, K. S. Thygesen, T. Vegge, et al., *J. Phys.: Condens. Matter* **2017**, *29*, 273002.
[62] L. Tsetseris, N. Kalfagiannis, S. Logothetidis, S. T. Pantelides, *Phys. Rev. B* **2007**, *76*, 224107.
[63] M. Ångqvist, W. A. Muñoz, J. M. Rahm, E. Fransson, C. Durniak, P. Rozyczko, T. H. Rod, P. Erhart, *Adv. Theory Simul.* **2019**, *2*, 1900015.